Supplementary information

Electron beam irradiation-assisted regulation of hydrophilic and hydrophobic coating method

Haozhe Li,[a] Keyan Sheng,[ac] Zhiyan Chen,[b] Shuai Hao,[b] Zijian Zhou,[a] Zhenyi Zhang,[a] Xinwen Liu,[a] Mianzhi Xiong,[a] Yanlong Gu[*b] and Jiang Huang[*a]

[a] State Key Laboratory of Advanced Electromagnetic Technology, Huazhong University of Science and Technology, Wuhan 430074, Hubei, PR China.
[b] Hubei Key Laboratory of Material Chemistry and Service Failure, School of Chemistry and Chemical Engineering, Huazhong University of Science and Technology, Wuhan 430074, Hubei, PR China.
[c] Huadian Electric Power Research Institute Co., LTD, Hangzhou 310030, China.

[*] Corresponding Authors: **Yanlong Gu** klgyl@hust.edu.cn

Jiang Huang jhuang@hust.edu.cn

Table of Contents

1. The electron irradiation accelerator utilized in this study

AB.10 (Wuxi El Pont, China) spanning a significant area, employs a concrete structure to provide radiation shielding and utilizes an acceleration tube measuring tens of meters in length to endow electrons with ample energy and high penetration depth. In this study, it was employed for the EBI grafting of hybrid materials G1-G5. EBLab 200 (Comet AG, Flamatt, Switzerland), with a coverage area of only two square meters, features a self-shielded and user-friendly design. However, it should be noted that the depth of penetration is at the micron level. In this study, it was utilized for accomplishing the curing process of e-HMS-PDMS coating.
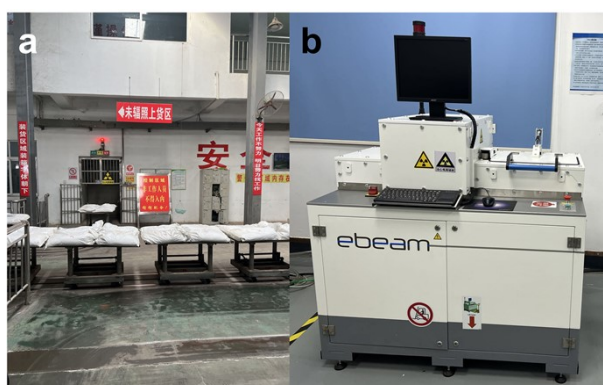
Fig. S1 The electron irradiation accelerator utilized in this study. (a) AB.10 10 MeV EBI accelerator; (b) EBLab 200 200 keV EBI accelerator.

2. Elemental analysis of G1 series of hybrid materials

Table S1. Elemental analysis results of G1 series of hybrid materials

Sample [a]	C (%)	H (%)	S (%)	N (%)
HMS-SH	15.5	2.7	11.0	0.9
G1-0	27.1	5.2	7.0	1.1
G1-1	28.8	5.3	6.7	1.6
G1-2	30.6	5.7	6.7	1.4
G1-3	31.9	5.8	6.5	1.6
G1-4	32.5	6.0	6.3	1.7
G1-5	33.1	6.1	6.1	1.6
G1-6	33.5	6.2	5.7	1.7

[a] Test condition: Elementar UNICUBE, CHNS model.

3. EDS diagram of G1 series of hybrid materials

Element	Wt %	At %
C	17.38	25.78
N	0.69	0.88
O	44.83	49.94
Si	27.92	17.72
S	7.37	4.09

Lsec: 153.6   0 Cnts   0.000 keV   Det: Octane Elect Super
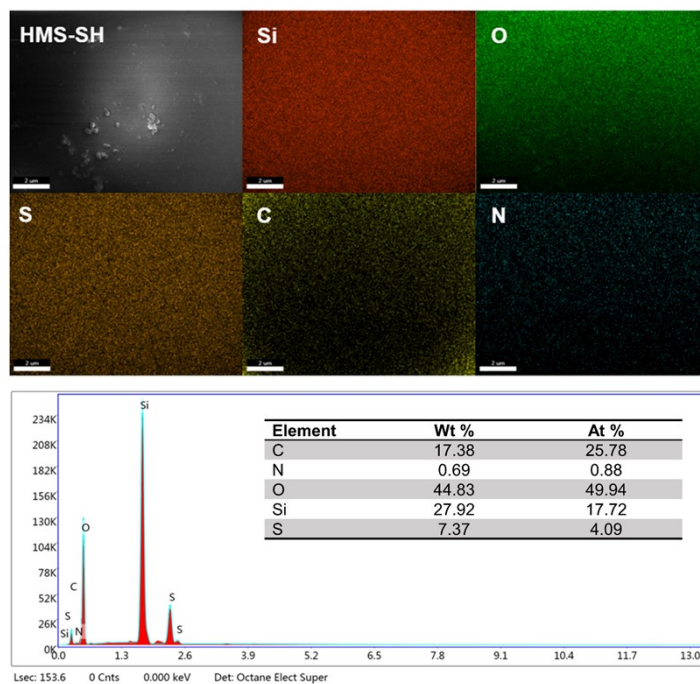
Fig. S2 The EDS mapping scan, elemental mass fraction, and atomic fraction analysis of HMS-SH material.

Element	Wt %	At %
C	21.72	31.22
N	0.92	1.14
O	44.46	47.98
Si	25.55	15.71
S	7.34	3.95

Lsec: 153.6   0 Cnts   0.000 keV   Det: Octane Elect Super
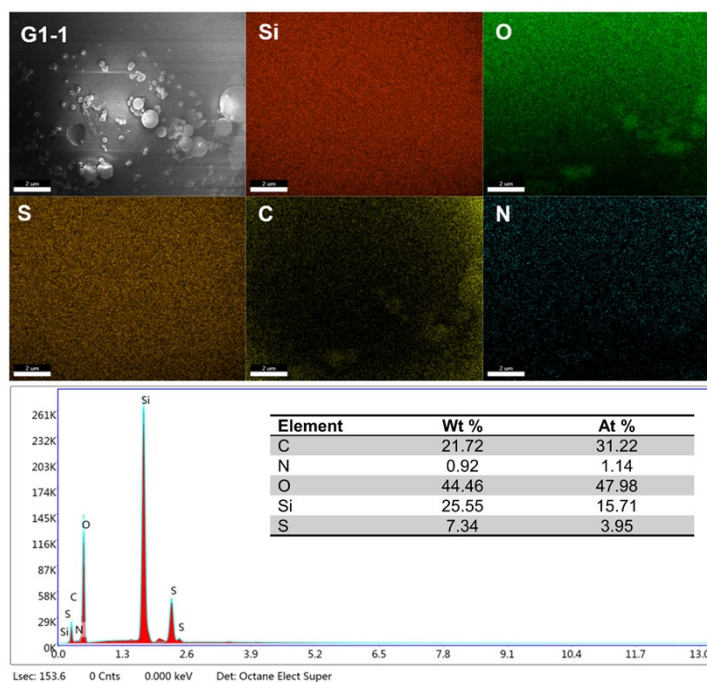
Fig. S3 The EDS mapping scan, elemental mass fraction, and atomic fraction analysis of G1-1 hybrid material.

Fig. S4 The EDS mapping scan, elemental mass fraction, and atomic fraction analysis of G1-3 hybrid material.
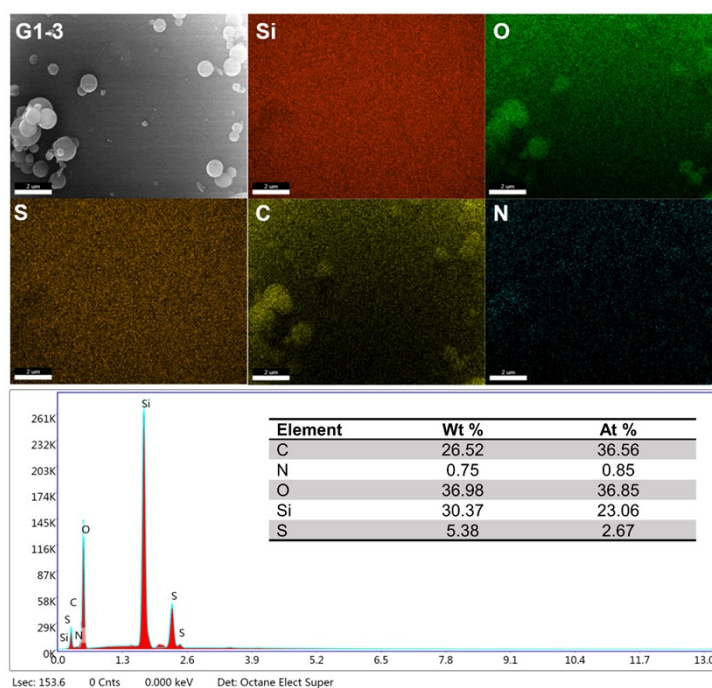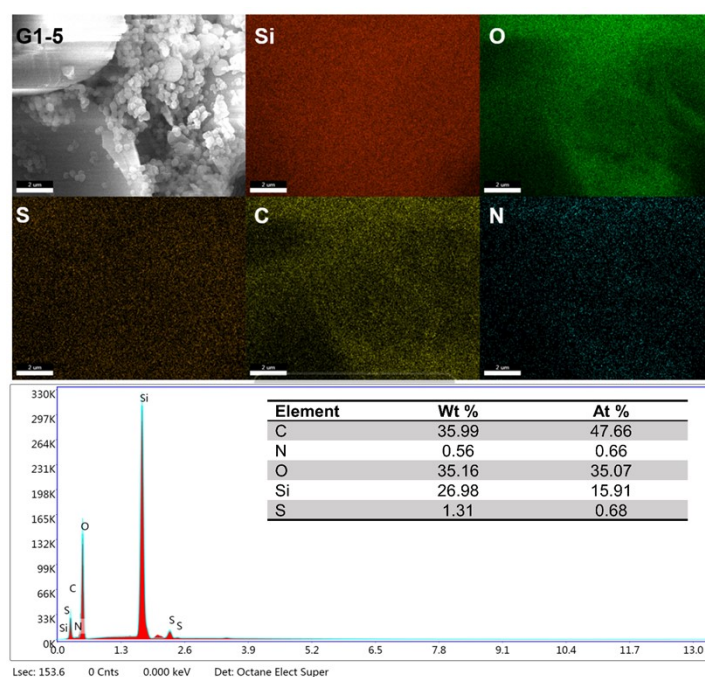

Fig. S5 The EDS mapping scan, elemental mass fraction, and atomic fraction analysis of G1-5 hybrid material.

4. Curing characteristics of the crosslinked PDMS evaluated from DSC

Table S2. Curing characteristics of the crosslinked PDMS evaluated from DSC

Sample	Tp (°C)	$\Delta H_{\infty(J/g)}$	T*	ΔH *
18% PDMS	-53.63	27.24	0.99	1.08
22% PDMS	-54.37	26.96	0.98	1.07
24% PDMS	-53.10	25.20	1.00	1.00
26% PDMS	-52.66	26.33	1.01	1.04
30% PDMS	-52.87	26.17	1.01	1.04

5. ATR-FTIR spectrum of crosslink PDMS coatings at different surface doses

The ATR-FTIR spectrum of 24% PDMS coatings under various irradiation doses is presented in Fig. S6 The peak at 2962 cm^{-1} and the faint peak at 1411 cm^{-1} correspond to the antisymmetric stretching vibration and bending vibration of end-group methane, respectively. These peaks exhibit significant overlap across different irradiation doses. Moreover, as illustrated in Fig. S6b, the intense absorption bands associated with Si-O-Si stretching vibrations at 1077 cm^{-1} and 1007 cm^{-1} are preserved[1]. DMS functions as a bridge to the PDMS cross-linking network, and the backlog enhances the intermolecular structure's compactness, which is also manifested in the Si-CH$_3$ rocking vibration absorption peak at 784 cm^{-1}.[2] Additionally, the wave number shifts from 784 to 788 cm^{-1}. Upon the formation of the radiation crosslinking network, the molecular structure of e-PDMS progressively compacts, which leads to the increase of the force constant of the chemical bond.[3]
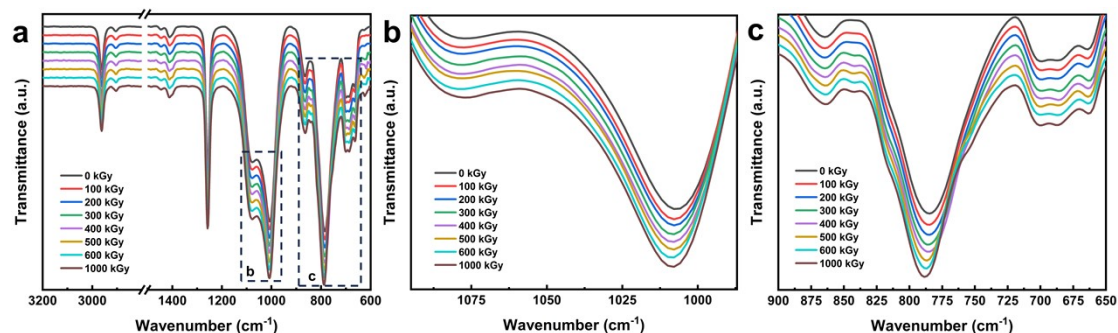

Fig. S6. The ATR-FTIR spectrum of 24% PDMS crosslinked at different irradiation

surface doses (a) complete spectrum (b and c) Partial details.

6. Hybrid material GC1 series prepared by chemical method

The preparation process of the Group chemical GC1 series of hybrid materials involves the following steps: HMS-SH (0.2 g), AIBN (0.82 g, 5 mmol), and 0.5 mol/L 3-sulfolene and Octadec-1-ene monomer solutions of varying volumes are added to a 25 mL pear-shaped bottle, resulting in a total volume of 5 mL of the modified liquid. The reaction takes place at 60°C for 8 hours. After filtration, the material is washed with acetonitrile (20 mL × 3) and ethanol (20 mL × 3), and then dried overnight at 80°C in a vacuum oven to obtain the GC1 series of hybrid materials. The hydrophilic and hydrophobic test results of the GC1 series coating are presented in Fig. S7.
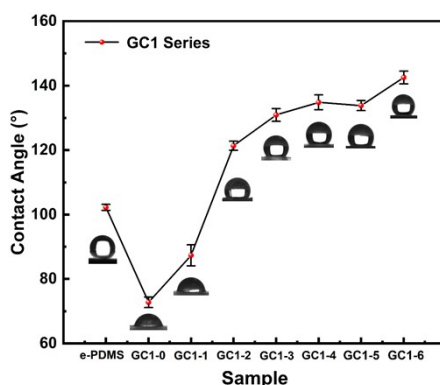
Fig. S7 The Coating contact angle test of GC1 series e-HMS-PDMS coatings.

7. Physicochemical characterization of G2-G4 series e-HMS-PDMS coatings

N, N'-Methylenebisacrylamide (MBAA) and octadec-1-ene were utilized for grafting monomers of G2 hybrid materials. MBAA, a thickening and binding agent in the textile industry,[4] is frequently employed as a crosslinking agent. As depicted in the FTIR spectra presented in Fig. S8a, the characteristic peaks and intensity fluctuations of octadec-1-ene exhibit similarities with those of G1. The emergence of new peaks at 1660 cm^{-1} and 1220 cm^{-1} indicates the presence of carbonyl stretching vibration and amide C-N stretching vibration,[5] respectively. Similarly, the single peak observed at

1530 cm^{-1} can be attributed to C-N-H bending vibration, thereby signifying the successful grafting of MBAA onto HMS. The intensity of this peak decreases with decreasing monomer concentration and completely disappears in the curve corresponding to G2-6. Fig. S8b illustrates the hydrophilicity of the G2 e-HMS-PDMS coatings. Given that MBAA is a hydrophilic compound possessing an amide functional group and displaying strong interaction with water molecules, the G2-0 coating exhibits pronounced hydrophilic properties. As the content of 1-octachene incrementally increases, the hydrophilicity of the coating correspondingly decreases, progressively transitioning towards hydrophobicity. The trend of hydrophilicity in G2 series coatings is like that of G1 series, but with a linear coefficient of determination of R^2 = 0.8517. In G2-5, the contact angle error on the same surface is as high as 16.4 degrees. According to the FSEM images, G2-3 e-HMS-PDMS coating is found to be interconnected and prone to agglomeration, leading to an uneven distribution of NPs on the coating's surface. This results in deviations in the surface characteristics of the same material.
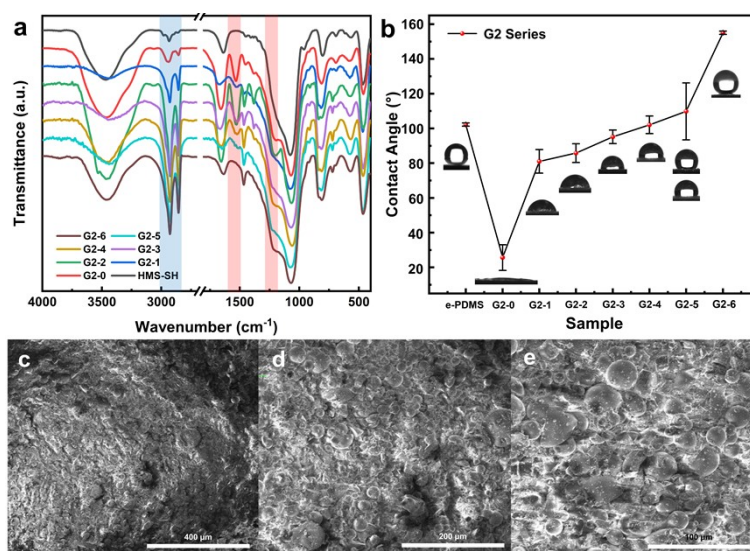
Fig. S8 The (a) FTIR spectra of G2 series additives; (b) contact angle test of G2 e-HMS-PDMS coating; (c d and e) FSEM images of G2-3 e-HMS-PDMS coating.

As illustrated in Fig. S9, vinylacetic acid and octadec-1-ene were chosen as the grafted monomers for the G3 series of hybrid materials additives. In Fig. S9a, a novel

peak emerges in the FTIR spectra corresponding to G3-0 to G3-5 at 1720 cm^{-1}, which represents the stretching vibration of the carbon-oxygen double bond.[6] This indicates that vinylacetic acid was successfully grafted. The intensity of the peak in the corresponding region gradually decreases. The linear determination coefficient of contact angle regulation, R^2=0.9980, for the G3 e-HMS-PDMS coatings in Fig. S9b surpasses that of all other monomers. Among the coatings studied, G3-0 exhibits a contact angle of 78°, indicating a slightly lower hydrophilicity compared to G1-0 and G2-0 coatings. The FSEM diagram reveals a distinct and scattered distribution of nanoparticles on the surface of the G3-3 coating, with well-defined boundaries between them; however, some agglomeration persists (Fig. S9e). Importantly, it is worth noting that such agglomeration is less prevalent compared to the G2 series.
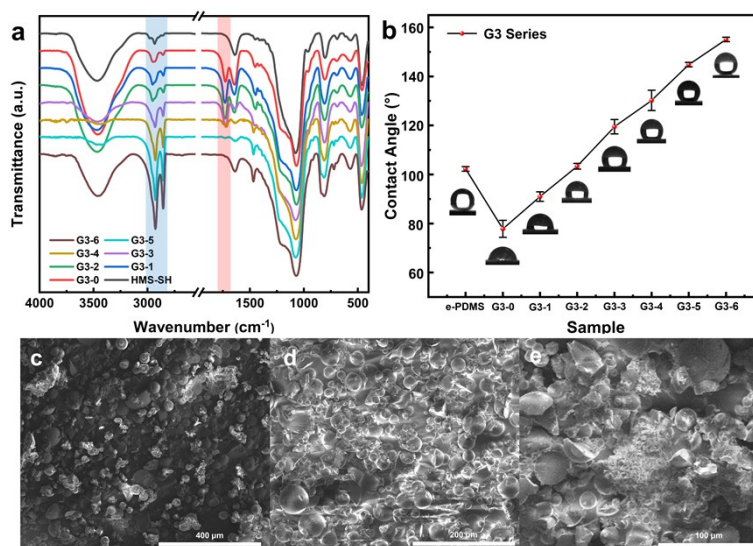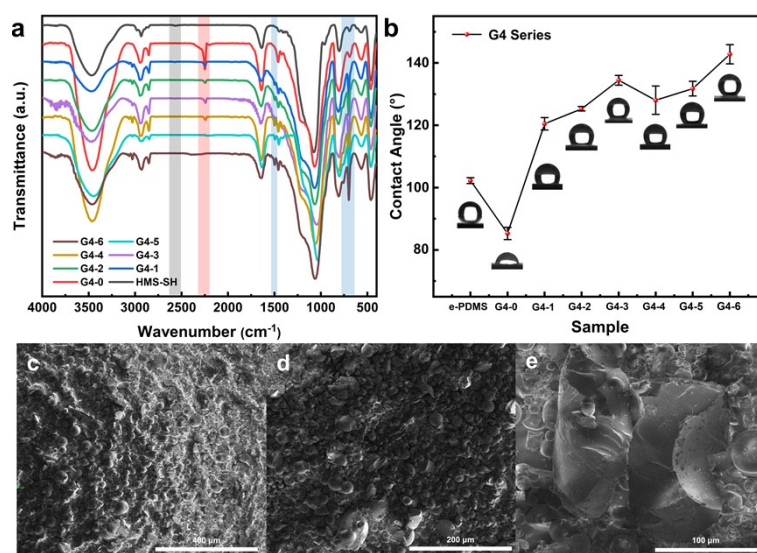

Fig. S9. The (a) FTIR spectra of G3 series additives; (b) contact angle test of G3 e-HMS-PDMS coating; (c d and e) FSEM images of G3-3 e-HMS-PDMS coating.

As illustrated in Fig. S10, acrylonitrile and styrene were chosen as the grafted monomers for the G4 series of hybrid materials additives. As revealed by the FTIR spectra analysis presented in Fig. S10a, the peak at 2248 cm^{-1} corresponds to the stretching vibration of the carbon-nitrogen triple bond in nitrile compounds. The emergence of new peaks at 700 cm^{-1} and 756 cm^{-1} in G4-1 to G4-6 signifies the bending vibration of the benzene ring,[7] while the faint peaks at 1450 cm^{-1} are attributed to the

stretching vibration of the aromatic ring. The intensity of these corresponding absorption peaks varies with the alteration of the monomer volume ratio. The hydrophilicity variation range of G4 series coatings, as illustrated in Fig. S10b, is minimal ranging from 85°to 142° and exhibits poor trend consistency with R^2=0.6815. This implies that the polarity difference among the selected monomers is insufficient for effective regulation of hydrophilicity. The FSEM diagram presents the surface morphology of the G4-3 coating. Except for the non-uniformity observed in some HMS materials during preparation, which is exemplified by the caking diagram (Fig. 10e), the overall morphology remains consistent and uniform.

Fig. S10. The (a) FTIR spectra of G4 series additives; (b) contact angle test of G4 e-HMS-PDMS coating; (c d and e) FSEM images of G4-3 e-HMS-PDMS coating.

The outcome of utilizing G5 series of hybrid materials additives, which incorporate acrylonitrile and octadec-1-ene as monomers, is presented in Fig. S11. The alteration in coating contact Angle is more conspicuous in comparison to the G4 series, and linear coefficient of determination R^2=0.8736. As the proportion of octadec-1-ene increases, the hydrophobicity of the coating is correspondingly enhanced, culminating in the attainment of superhydrophilicity. The investigations involving diverse monomers demonstrate that the grafting of distinct monomers yields varying effects on the surface properties of coatings. When employing this grafting method, it is

imperative to comprehensively consider the desired surface properties and select suitable monomers accordingly.
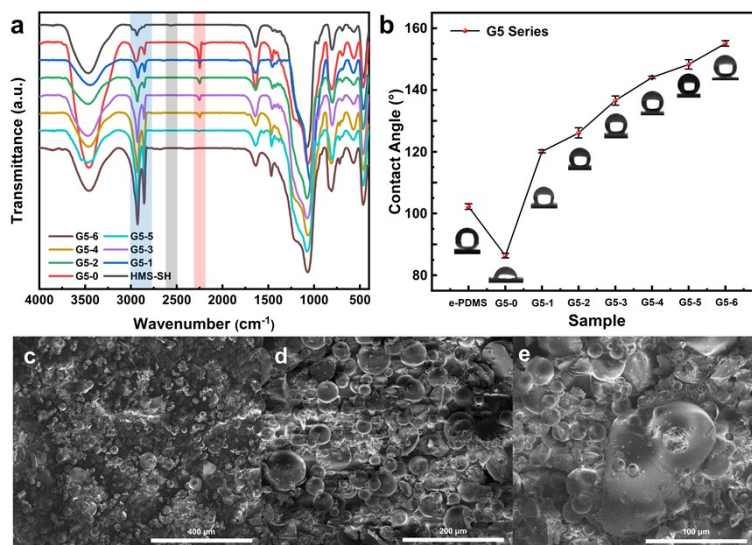
Fig. S11. The (a) FTIR spectra of G5 series additives; (b) contact angle test of G5 e-HMS-PDMS coating; (c d and e) FSEM images of G5-3 e-HMS-PDMS coating.

8. XRD analysis of samples grafted with single monomers

To investigate the impact of diverse monomers on the properties of HMS hybrid materials, XRD analysis was performed on samples grafted with single monomers selected in this study. As depicted in Fig. S12, the peak diminished at 2.4° post-grafting, with the HMS material grafted with styrene exhibiting the most prominent attenuation. Concurrently, the amorphous organic peak at 22° was amplified. Notably, the enhancement of the NP grafted with octadec-1-ene was the most pronounced.
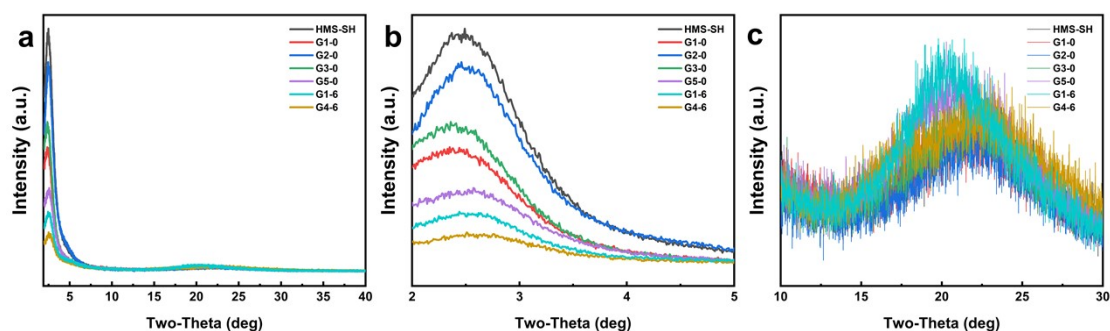
Fig. S12 The XRD patterns of monofunctional hybrid materials: (a) 2-40 degrees; (b) 2-5 degrees; (c) 10-30 degrees.

9. Particle size and zeta potential of G2-G5 hybrid materials

**Table S3.** Particle size and zeta potential of G2-G5 hybrid materials

Sample [a]	Z-average Size	PDI	Zeta-potential (mV)
HMS-SH	12470	0.320	-33.8
G2-0	33436	0.504	4.7
G2-1	31620	0.523	2.2
G2-2	20533	0.453	0.9
G2-3	18502	0.395	1.6
G2-4	19322	0.402	3.7
G2-5	21414	0.411	-21.6
G2-6	14517	0.474	-26.8
G3-0	13442	0.362	-39.4
G3-1	13591	0.370	-35.4
G3-2	13652	0.374	-36.5
G3-3	13950	0.392	-34.8
G3-4	14233	0.367	-32.4
G3-5	14620	0.418	-30.2
G3-6	14517	0.474	-26.8
G4-0	12399	0.377	-29.8
G4-1	11620	0.355	-25.0
G4-2	12590	0.373	-27.0
G4-3	14687	0.352	-37.6
G4-4	12200	0.323	-40.2
G4-5	12232	0.327	-43.6
G4-6	12650	0.360	-45.4
G5-0	12399	0.377	-29.8
G5-1	14566	0.360	-27.6
G5-2	15927	0.402	-27.4
G5-3	14658	0.432	-25.0
G5-4	16600	0.459	-27.6
G5-5	13660	0.402	-26.1
G5-6	14517	0.474	-26.8

[a] Test condition: BeNano180Zeta, 25 °C, deionized water as the dispersive medium, the parallel test is averaged three times.

10. The TEM image of G1 series hybrid materials

The HMS series microspheres synthesized in this study are prepared using tetraethyl orthosilicate (TEOS) and (3-mertopropyl) trimethoxysilane as silicon sources, with hexylamine serving as the template agent. Hexylamine is employed to induce pore formation during early silicon source guidance, which is subsequently removed through Soxhlet extraction after hydrolysis and condensation. The resulting polymer forms a shell structure around the template agent, leading to the hollow center of the microspheres.

To confirm their hollowness, transmission electron microscope (TEM) characterization was conducted on parts of both HMS-SH and G1 series microspheres, with Fig. S13 displaying the results. Across different grafting rates from HMS-SH to G1 series, numerous surface layer pore structures were observed on all silicon microspheres, exhibiting a relatively uniform distribution that contributes to their high specific surface area. As depicted in Fig. S13, the center of each silicon microsphere exhibits a distinct hollow feature along with an evident shell structure. The silicon microspheres prepared under similar reaction conditions have been verified to possess hollow structures, as reported.[8, 9, 10] In conclusion, we posit that these silicon microspheres possess a hollow architecture.
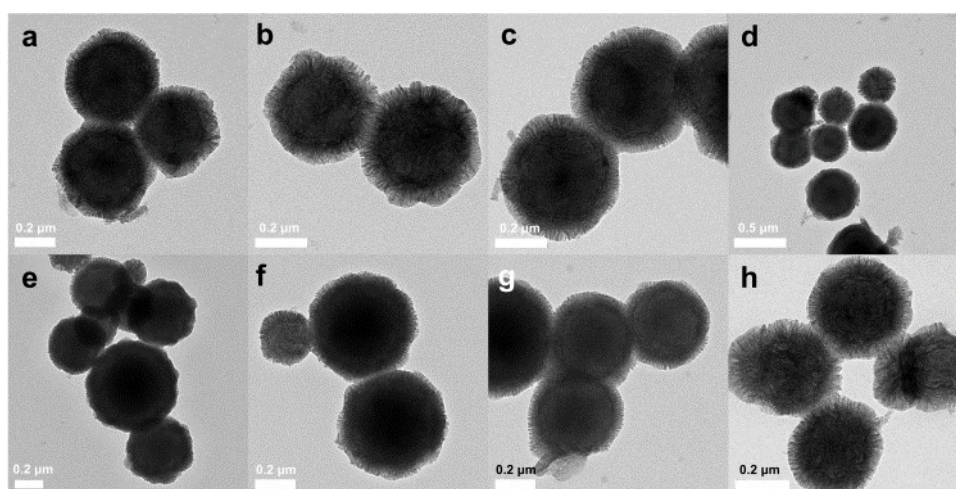
Fig. S13 The TEM image of (a and b) HMS-SH; (c and d) G1-0; (e and f) G1-3; (g and h)

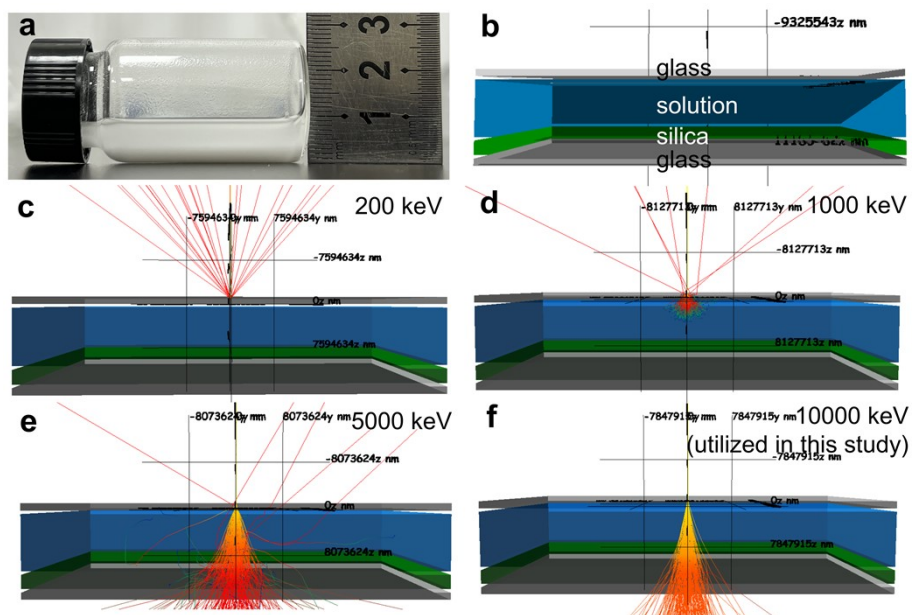## 11. The Monte Carlo simulation of EBI grafting and curing process

To verify the penetration depth of electron beam grafting, Monte Carlo simulation was employed to simulate the energy attenuation and penetration of electrons incident on the sample bottle with varying energies. The Monte Carlo method is employed to simulate the stochastic interaction between an electron beam and matter, enabling its application in energy deposition simulation, radiation effect study, material characterization, and semiconductor device simulation. CASINO is a software specifically designed for simulating the trajectory and interaction of electrons within solids. Widely utilized in physics, materials science, and electronic engineering fields, it offers extensive parameter customization options as well as result analysis capabilities to facilitate a comprehensive understanding of material properties and behavior.

The simulation model was based on an actual 20 mL sample bottle. Electrons were directed from top to bottom, initially penetrating a 1 mm thick glass layer, traversing through an air section, penetrating an 8 mm thick modified solution layer, subsequently entering a 2 mm thick HMS microsphere layer, and finally passing through another 1 mm thick glass layer. Monte Carlo simulation software CASINO v3.3 was utilized for this purpose. The number of electrons used in the simulation was set at 1000 while adjusting their initial energy according to the input element composition and corresponding density of different thicknesses within the model layers.

The simulation results are depicted in Fig S14. If using 200 keV electrons, due to their low energy level they can hardly penetrate the first glass layer and instead get reflected into the upper space. With 1000 keV electrons, they can penetrate the first glass layer but rapidly decay upon entering the solution layer resulting in limited efficiency. Electrons possessing an energy level of 5000 keV can effectively penetrate throughout the entire sample bottle; however, some electrons still experience

reflection when traversing each individual layer. The chosen electron beam energy for this study is set at 10,000 keV which not only enables complete penetration of all layers within the sample bottle but also exhibits minimal attenuation in electron energy thereby significantly influencing the entire reaction system.

Fig. S14 Monte Carlo simulation results of EBI grafting process: (a) Physical photograph; (b) Modeling schematic diagram; (c) 200 keV energy; (d) 1000 keV energy; (e) 5000 keV energy; (f) 10000 keV energy electron.

The process of electron beam curing was investigated through Monte Carlo simulation in Fig. S15. A model was established based on the actual conditions. A coating solution containing additives, with a thickness of 250 microns, was applied onto a silicone rubber substrate measuring 3 mm in thickness. The incident energy of electrons was determined to be 200 keV. As shown in Fig. S15b, the electron energy is significantly attenuated upon interaction with the coating solution. Combining this observation with Fig. S15c, it can be concluded that the maximum penetration depth for this energy is 400 microns, allowing for complete curing by fully penetrating the coating layer.
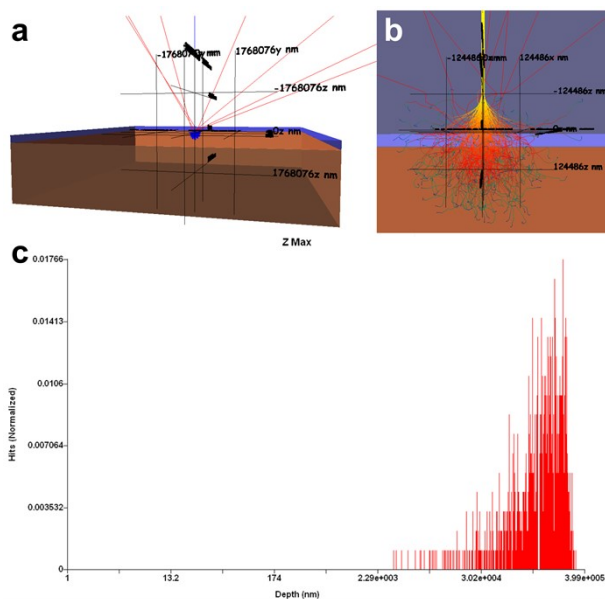
Fig. S15 Monte Carlo simulation results of EBI curing process: (a) Modeling schematic diagram; (b) Local amplification of electron penetration; (c) Electron penetration depth chart.

12. EDS mapping of G1 series hybrid materials (Small magnification）

To validate the spherical morphology of HMS microspheres and the uniformity of grafting on their surfaces, EDS surface scanning was conducted at a lower magnification, and the results are presented in Fig. S16 to Fig. S18. Comparing with the localized magnification shown in Fig. S2 to Fig. S5, it is evident that the distribution of elements in the G1 series of silicon hybrid materials exhibits a spherical outline and relatively even surface distribution. However, due to potential interference from conductive adhesive and other factors, caution should be exercised when interpreting quantitative analysis results for element composition.
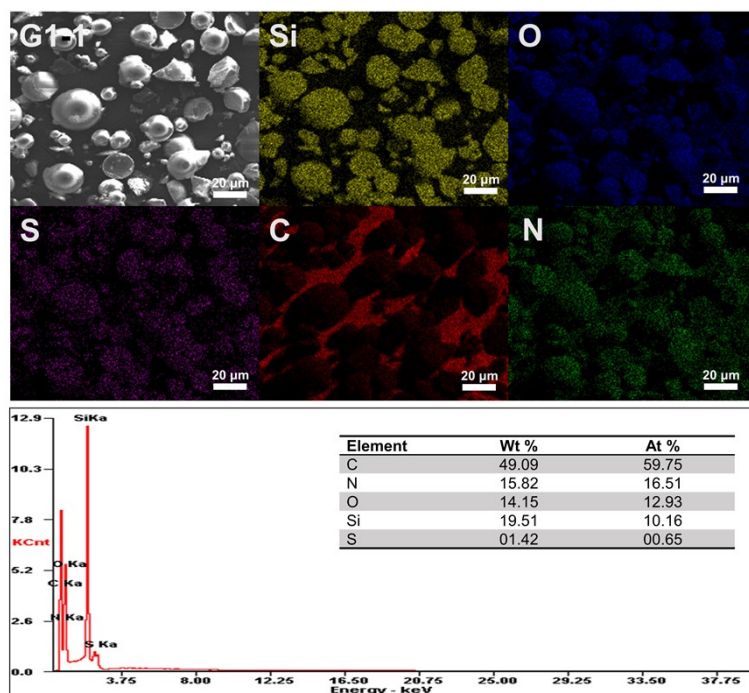
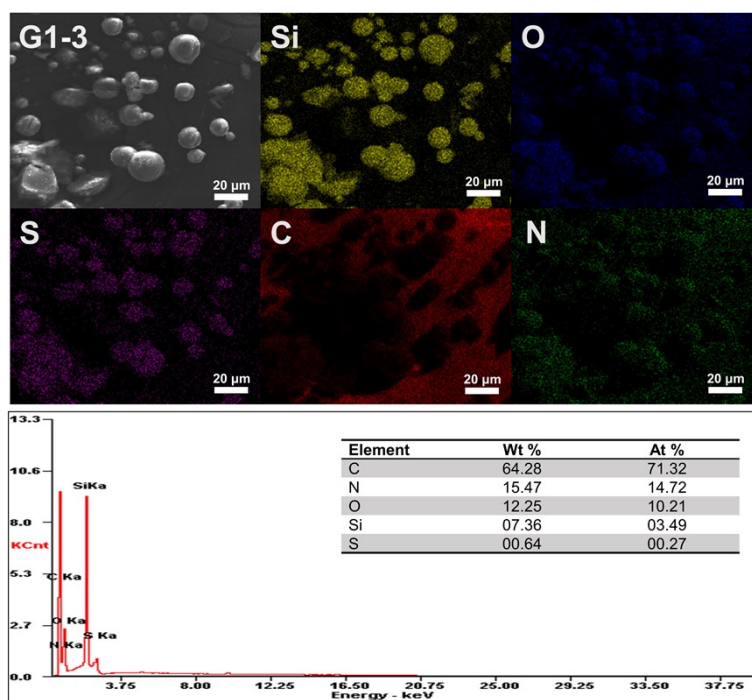**Fig. S16** The EDS mapping scan images of the hybrid materials of G1-1.

Element	Wt %	At %
C	49.09	59.75
N	15.82	16.51
O	14.15	12.93
Si	19.51	10.16
S	01.42	00.65

Fig. S17 The EDS mapping scan images of the hybrid materials of G1-3.

Element	Wt %	At %
C	64.28	71.32
N	15.47	14.72
O	12.25	10.21
Si	07.36	03.49
S	00.64	00.27

Element	Wt %	At %
C	62.37	70.20
N	15.14	14.61
O	12.16	10.28
Si	09.41	04.53
S	00.92	00.39
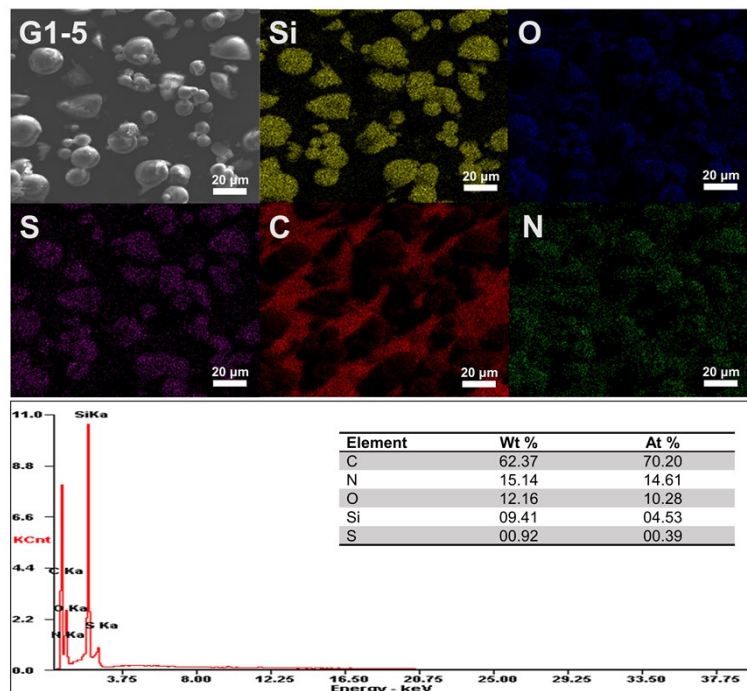
**Fig. S18** The EDS mapping scan images of the hybrid materials of G1-5.

### 13. Contact Angle of pure 24%PDMS at different doses

To determine the effect of electron beam irradiation on the hydrophilicity of PDMS components in the coating, 200 keV electron beams were used to cure PDMS with a purity of 24% at different doses, and their surface properties were carefully examined. As shown in Fig. S19. In the absence of any electron beam, the contact Angle of 24% PDMS is about 112°; However, as the radiation dose increases, it gradually drops to about 103° and eventually stabilizes at a dose of 300 kGy. Even when the dose was increased to 1050 kGy, the contact Angle remained stable at about 104°. These findings clearly show that electron beam irradiation has a negligible effect on the surface properties of pure PDMS, while the differences in hydrophilicity and hydrophobicity between e-HMS-PDMS coatings are attributed to different monomer grafting rates of the additives.
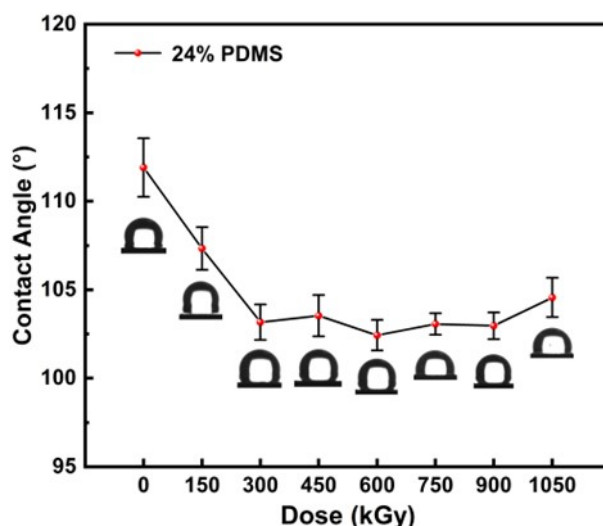
Fig. S19 Contact angles of 24%PDMS coatings at different EBI doses.

14. Effect of additive content on hydrophilicity of coatings

In this coating preparation method described herein, PDMS and DMS are cross-linked under electron beam induction to serve as a bonding layer between the silicone rubber substrate and silicon microsphere additives. The surface characteristics of the coating primarily depend on those of the additives. To ensure this, a minimum of 20 wt% additive should be included. For improved coating stability, we opted to include 25 wt% silicon microsphere additives in this study.
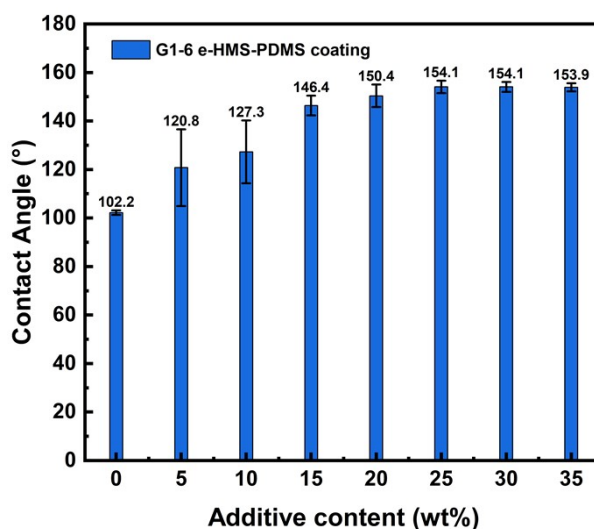
Fig. S20 Effect of additive content on hydrophilicity of coatings

References

1. Y. Pan, G. Chen, J. Liu, J. Li, X. Chen, H. Zhu, G. Liu, G. Zhang and W. Jin, PDMS thin-film composite membrane fabricated by ultraviolet crosslinking acryloyloxy-terminated monomers, *J. Membrane Sci.*, 2022, **658**, 120763.

2. D. Maji, S. K. Lahiri and S. Das, Study of hydrophilicity and stability of chemically modified PDMS surface using piranha and KOH solution, *Surf. and Interface Anal.*, 2012, **44**, 62-69.

3. M. N. Shah, N. H. Patel, D. D. Shah and P. K. Mehta, FTIR: Important tool to investigate the chemical bond formation in the polycrystalline xBaTiO3-(1-x)BiFeO3, *Mater. Today: Proceedings*, 2021, **47**, 616-620.

4. M. Kubota, T. Mochizuki, S. Yamashita, H. Kita and H. Tokuyama, Water vapor adsorption on poly(N-isopropylacrylamide) gel cross-linked with *N, N'*-methylenebisacrylamide, *Mater. Today Commun.*, 2020, **22**, 100804.

5. F. Nishio, I. Hirata, K. Nakamae, K. Tsuga and K. Kato, Mucoadhesion of polyamphoteric hydrogels synthesized from acrylic acid and N,N-dimethylaminopropyl acrylamide, *Int. J. Adhes. Adhes.,* 2021, **104**, 102746.

6. Z. Shao, B. Tan, C. Su, X. Zan, X. Song and H. Wang, Study on the variation in key functional groups of coal and the mechanism of CO and CO_2 generation under the thermal effect of lean-oxygen conditions, *Fuel*, 2024, **357**, 130061.

7. A. I. Fishman, A. E. Klimovitskii, A. I. Skvortsov and A. B. Remizov, The vibrational spectra and conformations of ethylbenzene, *Spectrochim. Acta A*, 2004, **60**, 843-853.

8. S. S. Yang, Z. Chen, T. Q. Chen, and C. Ya. Fu, Hollow Mesoporous Silica Nanoparticles Decorated with Cyclodextrin for Inhibiting the Corrosion of Mg Alloys, *ACS Appl. Nano Mater*. 2020, **3**, 4542–455.

9. J. Hu, W. Shan, W. Zhang, Y. Zhang and Y. Tang, Morphological diversity of dual meso-structured HMS and their transformation process, *Micropor. Mesopor. Mat.,* **2010**, 129, 210-219.

10. Sh. Ghasemi, Z. Jomeh Farsangi, A. Beitollahi, M. Mirkazemi, S.M. Rezayat, S. Sarkar, Synthesis of hollow mesoporous silica (HMS) nanoparticles as a candidate for sulfasalazine drug loading, *Ceram. Int.*, **2017**, 43, 11225-11232.